Precise tailoring of the crystal size distribution by controlled growth and continuous seeding from impinging jet crystallizers

Xing Yi Woo,[d] Reginald B. H. Tan[bc] and Richard D. Braatz*[ae]

Received 12th September 2010, Accepted 31st October 2010
DOI: 10.1039/c0ce00637h

The desired bioavailability and the method of drug administration and delivery can require stringent control on the crystal size distribution. Optimal control strategies are proposed to manufacture crystals with a targeted size distribution by combining controlled seeding by impinging jet crystallization with a batch crystallizer operating at a controlled constant growth rate. The same strategies apply if the impinging jet crystallization is replaced by any process equipment that can continuously provide crystal seeds, typically through the application of high supersaturation, to the batch crystallizer. Limitations to the achievable crystal size distributions and sensitivity to process operations are analyzed. Simulation results indicate that one of the strategies has promise for manufacturing pharmaceutical crystals of a desired size distribution.

Introduction

The control of crystal size distribution (CSD) in a batch or continuous crystallization process is critical for efficient downstream processing[6,22] and satisfying company internal and governmental regulatory demands for product consistency.[41] In addition, the desired bioavailability and the method of drug administration and delivery, for example pulmonary delivery, can demand stringent control on the crystal size distribution.[37,42,46]

The control of a batch crystallization process typically involves following a pre-determined optimal cooling or anti-solvent addition trajectory,[30,43,45,48,54,38] or using feedback control, with on-line monitoring, to maintain a constant supersaturation during the crystallization process.[12,14,27,55] Reviews of various types of crystallization control strategies are available.[13,51,39,52] The mass, size distribution, and addition time of the seed crystals have a significant impact on the final crystal size distribution such that the quantity and distribution of the seed crystals can be optimized for a given product quality.[7,8,17,18,23,28,44,48,4,25] Usually these control and optimization strategies are targeted towards the production of large crystals of narrow unimodal size distribution for efficient downstream processing.

The large crystals typically produced from batch crystallizers require further milling to increase the surface area to meet dissolution, tableting, and bioavailability requirements. The undesirable effects from milling[1,3] motivates the development of crystallization processes to directly produce small particles with narrow distribution. Current state-of-the-art includes impinging jet crystallization,[2,11,19,26,32,34] and crystallization using supercritical fluids.[21,36,40,46] The development of these processes to their full potential requires a thorough understanding of the processes, which can be achieved by modeling[16,33] and experimentation combined with imaging, light scattering, and other measurement techniques.[5] This paper will show how to use this understanding to develop an optimal control strategy to precisely tailor the crystal size distribution specific to the bioavailability requirements of an active pharmaceutical ingredient (API).

This paper proposes three control strategies whose goal is to produce crystals with a *target crystal size distribution* (CSD), that are combinations of optimal control and an impinging jet crystallizer. Analysis of the first control strategy indicates that the CSDs obtainable by an impinging jet crystallizer by itself are limited. However, the other two control strategies that combine the impinging jet with an aging vessel controlled at constant supersaturation show greatly enhanced controllability of the CSD compared to past academic studies and current industrial practice. Simulation results for the Lovastatin system indicate that even square and multimodal distributions can be obtained, with selected size ranges and distribution peaks and widths. Sensitivity and controllability analyses indicate a high controllability of the CSD with moderate to low sensitivity to disturbances.

Trying to tailor CSD by combining crystals produced at different jet velocities

Based on simulation studies,[53] the crystal size distributions obtained from confined impinging jets are shown in Fig. 1. Fig. 2 shows the increase in the mean crystal size and distribution width with a decrease in jet velocity.

Optimization formulation

The crystal size distributions obtained by varying the jet velocity of a single impinging jet or multiple impinging jets in parallel can

[a]*Department of Chemical and Biomolecular Engineering, University of Illinois at Urbana-Champaign, 600 South Mathews Avenue, Urbana, IL, 61801. E-mail: braatz@mit.edu; Fax: +617-258-0546; Tel: +617-253-8410*
[b]*Department of Chemical and Biomolecular Engineering, National University of Singapore, 4 Engineering Drive 4, Singapore 117576*
[c]*Institute of Chemical and Engineering Sciences, 1 Pesek Road, Jurong Island, Singapore 627833*
[d]*Genome Institute of Singapore, 60 Biopolis Street, #02-01, Genome, Singapore 138672*
[e]*Department of Chemical Engineering, Massachusetts Institute of Technology, 77 Massachusetts Avenue, Cambridge, MA, 02139*

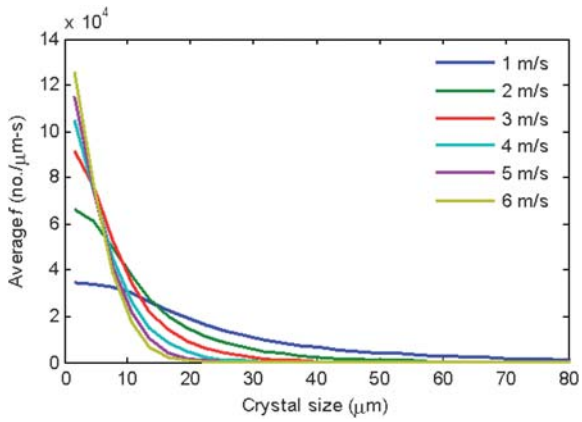

Fig. 1 Simulated crystal size distribution of Lovastatin from confined impinging jets.

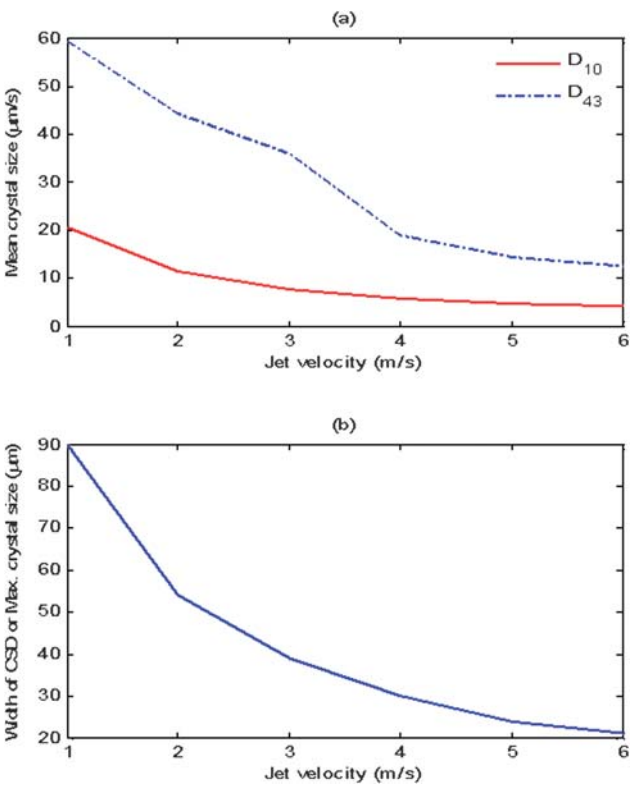

Fig. 2 Effect of impinging jet velocity on **(a)** the mean crystal size and **(b)** the width of the distribution (equals to maximum crystal size since minimum crystal size is 0 μm). The maximum crystal size is defined as the crystal size when f/μ_0 becomes $< 1 \times 10^{-3}$.

be combined to tailor the crystal size distribution. The proportions of crystals produced at each jet velocity can be obtained by solving the optimization:

$$\min_{w_i \geq 0} \left\| F(L) - \sum_i w_i f_i(L) \right\| = \min_{w_i \geq 0} \int_0^\infty \left[F(L) - \sum_i w_i f_i(L) \right]^2 \mathrm{d}L \tag{1}$$

where $F(L)$ is the target crystal size distribution, $f_i(L)$ is the crystal size distribution for a given jet velocity v_i, w_i is the weight of the corresponding crystals, and $\|\cdot\|$ is an appropriately defined norm. The weight w_i is proportional to the time running the impinging jet at velocity v_i, for operations in which the temperature is constant. In this formulation, the set of jet velocities are fixed while the weights of the crystal size distribution corresponding to each jet velocity are optimized. A nearly continuous range of jet velocity can be considered by including a very large number of velocities in the formulation.

Eqn (1) can be expressed as

$$\min_{w_i \geq 0} \left\{ \int_0^\infty [F(L)]^2 \mathrm{d}L - 2 \sum_i w_i \int_0^\infty f_i(L) F(L) \mathrm{d}L + \sum_i \sum_j w_i w_j \int_0^\infty f_i(L) f_j(L) \mathrm{d}L \right\} \tag{2}$$

which can be solved with a quadratic programming solver (*e.g.*, "quadprog" in Matlab) that can be initialized by the unconstrained solution of (2) to produce (3) [on the top of the next page]:

Obtainable crystal size distributions

Fig. 3 shows the crystal size distributions obtained based on two different target distributions and the respective weights of crystals for six different jet velocities. While one target CSD could be obtained approximately by combining crystals from operating the impinging jet at 2 and 3 m s^{-1}, the second target CSD could not be obtained. To gain some insight into this, the CSDs obtainable by combining crystals from an impinging jet operating at the six different velocities are quantified in Fig. 4. The maximum crystal size, or width of the distribution, is specified by the crystals obtained at the lowest jet velocity. From Fig. 1 it is seen that this holds regardless of how many different inlet velocities are used within the range of operation (1–6 m s^{-1}).

Another general observation is that the shape of the overall CSD is fixed to be monotonically decreasing since all of the CSDs produced by the impinging jet are monotonically decreasing. Combining crystals from different inlet velocities does not give a significantly larger variety of CSDs than obtainable by operating the impinging jet at one inlet velocity (see Fig. 4b). The second target CSD in Fig. 3b is not monotonically decreasing and so can not be obtained by combining crystals from different inlet velocities. Although this study utilized CSDs from a simulation model, experimental studies also have reported similar monotonically decreasing CSDs for the full range of inlet velocities,[31] in which case there is little control over the target CSD by combining crystals at different inlet velocities.

Tailoring CSD by optimal seeding into an aging vessel

An impinging jet crystallizer can be used to tailor the crystal size distribution by sending the crystals to an aging vessel to grow.

Optimization formulation

In this approach, crystals of the narrowest distribution (jet velocity = 6 m s^{-1}) from the impinging jet are quenched, filtered, and dried. Subsequently, various weights of crystals are dropped

$$\begin{bmatrix} w_1' \\ \vdots \\ w_{i,\max}' \end{bmatrix} = \begin{pmatrix} \int_0^\infty f_1(L)f_1(L)\mathrm{d}L & \cdots & \int_0^\infty f_1(L)f_{i,\max}(L)\mathrm{d}L \\ \vdots & \ddots & \vdots \\ \int_0^\infty f_{i,\max}(L)f_1(L)\mathrm{d}L & \cdots & \int_0^\infty f_{i,\max}(L)f_{i,\max}(L)\mathrm{d}L \end{pmatrix}^{-1} \begin{bmatrix} \int_0^\infty f_1(L)F(L)\mathrm{d}L \\ \vdots \\ \int_0^\infty f_{i,\max}(L)F(L)\mathrm{d}L \end{bmatrix} \quad (3) \tag{3}$$

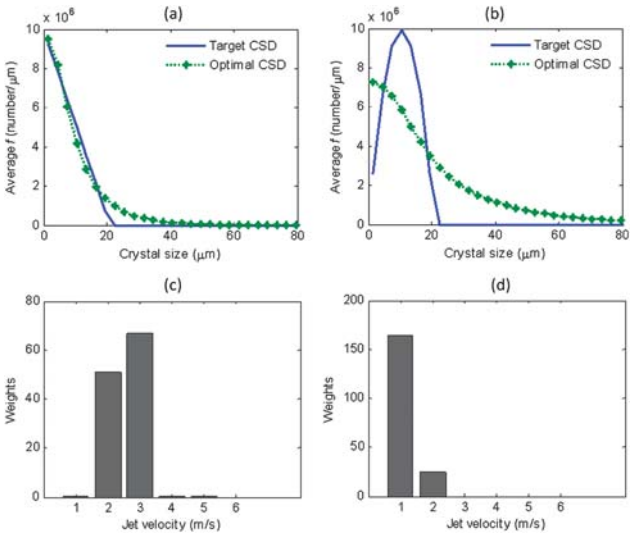

Fig. 3 Crystal size distributions obtained by optimally combining crystals obtained from impinging jets operating at six inlet velocities for **(a)** monotonic and **(b)** nonmonotonic target CSDs, with corresponding optimal combinations of continuous seeding in **(c)** and **(d)**, respectively.

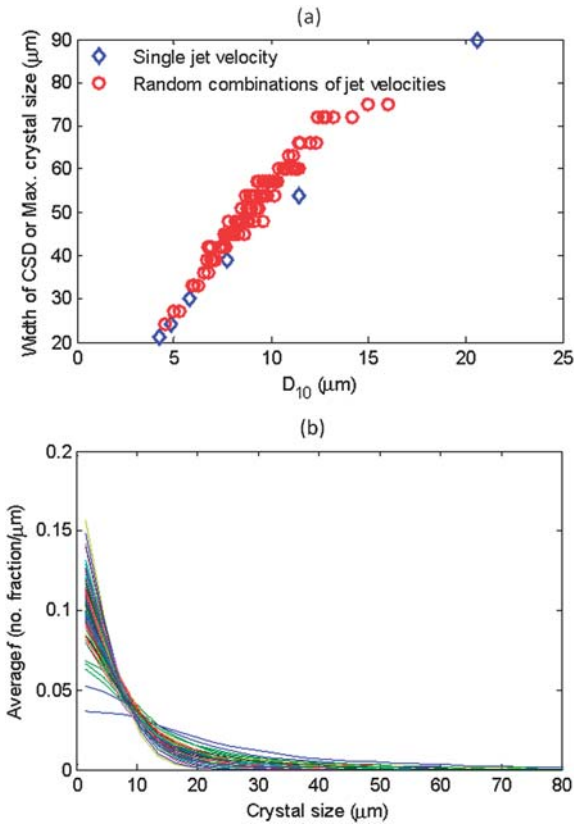

Fig. 4 **(a)** Widths of crystal size distribution and mean crystal sizes, and **(b)** crystal size distributions obtainable from single jet velocities or by combining crystals from impinging jets operating at jet velocities between 1 m s^{-1} to 6 m s^{-1}.

into an aging vessel for further crystal growth for various times. In other words, this strategy optimizes a seeding time profile based on the target distribution, using seeds of narrow distribution, for the operation of a batch crystallizer confined to operate under constant growth conditions:

$$\min_{\substack{w_i \geq 0 \\ t_{\mathrm{grow},i} \geq 0}} \left\| F(L) - \sum_i w_i f_{\mathrm{grow},i}(L) \right\| = \min_{\substack{w_i \geq 0 \\ t_{\mathrm{grow},i} \geq 0}} \left\| F(L) - \sum_i w_i f\left(L - Gt_{\mathrm{grow},i}\right) \right\| \quad (4) \tag{4}$$

where $f_{\mathrm{grow},i}$ is the crystal size distribution of the crystals after growing for the time interval $t_{\mathrm{grow},i}$. The time to drop in the crystals, $t_{\mathrm{drop},i}$, of weight w_i can be determined from the total batch time for the crystallizer, t_{batch}:

$$t_{\mathrm{drop},i} = t_{\mathrm{batch}} - t_{\mathrm{grow},i} \quad (5) \tag{5}$$

The minimum batch time is given by $t_{\mathrm{batch}} = \max_i\{t_{\mathrm{grow},i}\}$.

To simplify the formulation, a constant growth rate, G, was used, which can be easily achieved by constant supersaturation control,[13,55] which is optimal or nearly optimal for most crystallizers.[20] In this case the term, $f(L - Gt_{\mathrm{grow},i})$, can be evaluated by shifting the crystal size distribution along the crystal size axis (that is, the method of characteristics[35]). In cases where secondary nucleation, agglomeration, and/or breakage cannot be avoided, a full population balance model that includes the relevant kinetics can be used to determine $f_{\mathrm{grow},i}$. Note that judicious control and adjustment of the supersaturation and agitation rates, as well as choice of solvents, can reduce the extent of secondary nucleation, agglomeration, and breakage.[12]

Eqn (4) is similar to the optimization formulation frequently used in the deconvolution of peaks in chromatograms,[47,49,50] which can be solved using any nonlinear least-squares optimization solver (*e.g.* "lsqonlin" in Matlab). Thus, eqn (4) can be re-written for least-squares optimization as

$$\min_{\substack{w_i \geq 0 \\ t_{\mathrm{grow},i} \geq 0}} \sum_{j=1}^{N} \left[F(L_j) - \sum_i w_i f_{\mathrm{grow},i}(L_j) \right]^2 \quad (6) \tag{6}$$

where $F(L_j)$ and $f_{\mathrm{grow},i}(L_j)$ are the cell-averaged population density discretized along the growth axis of the crystal. The nonlinear solver can be initialized by the unconstrained solution of (3) with the approximation $f(L) = \alpha\delta(L)$, where $\delta(L)$ is the Dirac delta function and α is a scalar:

$$\begin{aligned}
&\min_{w_i}\left\| F(L) - \sum_i w_i\alpha\delta\left(L - Gt_{\mathrm{grow},i}\right)\right\| \\
&= \min_{w_i} \int_0^\infty \left[F(L) - \sum_i w_i\alpha\delta(L - Gt_{\mathrm{grow},i})\right]^2 \mathrm{d}L \\
&= \min_{w_i}\left\{ \int_0^\infty [F(L)]^2\mathrm{d}L - 2\alpha\sum_i w_i \int_0^\infty \delta\left(L - Gt_{\mathrm{grow},i}\right)F(L)\mathrm{d}L \right. \\
&\qquad \left. +\alpha^2\sum_i\sum_j w_iw_j\int_0^\infty \delta\left(L - Gt_{\mathrm{grow},i}\right)\delta\left(L - Gt_{\mathrm{grow},j}\right)\mathrm{d}L\right\} \\
&= \min_{w_i}\left\{\int_0^\infty [F(L)]^2\mathrm{d}L - 2\alpha\sum_i w_iF\left(Gt_{\mathrm{grow},i}\right) + \alpha^2\sum_i w_i^2\right\}
\end{aligned} \tag{7}$$

$$\begin{aligned}
&\frac{\mathrm{d}}{\mathrm{d}w_i}\left\{\int_0^\infty [F(L)]^2\mathrm{d}L - 2\alpha\sum_i w_iF\left(Gt_{\mathrm{grow},i}\right) + \alpha^2\sum_i w_i^2\right\} = 0 \\
&\qquad \Rightarrow \quad -2\alpha F\left(Gt_{\mathrm{grow},i}\right) + 2\alpha^2 w_i = 0
\end{aligned} \tag{8}$$

$$\Rightarrow\ w_i = (1/\alpha)F(Gt_{\mathrm{grow},i}) = (1/\alpha)F(G(t_{\mathrm{batch}} - t_{\mathrm{drop},i})) \tag{9}$$

Hence a plot of the optimal weights w_i as a function of the drop time should look like a "flipped" version of the target crystal size distribution. In addition, $t_{\mathrm{grow},i}$ can be initialized by:

$$\begin{aligned}
t_{\mathrm{grow},i} = L_i/G \quad \text{and} \quad L_i = \frac{i-1}{I-1}(L_{\max} - L_{\min}) \\
+ L_{\min},\ \text{for i} = 1,\ 2,\ \ldots,\ I,
\end{aligned} \tag{10}$$

where I is the number of times to drop in the seed crystals, and $L_{\min}$ and $L_{\max}$ are the minimum and maximum crystal size of the target distribution, $F(L)$.

Obtainable crystal size distributions

Fig. 5 shows the optimal crystal size distribution and times for dropping in the crystals with the corresponding weights for two target distributions. The growth rate was 2 μm min^{-1}. Fig. 5 illustrates how this method allows great flexibility in specifying the shape of the distribution in addition to the crystal size and the width of the distribution. This approach has the capability of tailoring any crystal size distribution of any shape, including flat-top and multi-modal distributions such as shown in Fig. 5, as long as the target CSD does not have characteristics narrower than the narrowest CSD produced by the impinging jet. More specifically, the CSD based on the optimal seeding profile will deviate from that of the target CSD when the width of the target CSD is narrower than the crystal size distribution from the impinging jets, and when there is a decrease in number density along the crystal size axis that is much sharper than that of any CSD produced by the impinging jet (see Fig. 6 for examples, focusing on where the deviations between the target and optimal CSD occur).

Tailoring CSD by optimal control of jet velocity

This section describes another strategy in tailoring the crystal size distribution by combining the operation of an impinging jet crystallizer with a batch aging vessel.

Optimization formulation

In this approach, the crystals from the impinging jet crystallizer are quenched (to freeze the crystal size distribution) and directly sent to an aging vessel. Similar to the previous strategy, the supersaturation in the aging vessel is controlled such that the growth rate remains constant. By varying the velocity from the impinging jets with time, the crystal size distributions that are added into the aging vessel varies with time, and can result in different product size distributions at the end of the aging run. Hence, this offers an opportunity to tailor the crystal size distribution towards a target distribution by optimizing the time-profile of crystal size distributions from the impinging jet crystallizer. In other words, this involves the optimal control of the jet velocity with time:

$$\min_{\substack{v_{\mathrm{jet}}(t) \\ \text{Eq. (12)}}} \int_0^\infty [F(L) - f_{\mathrm{end}}(L)]^2\mathrm{d}L \tag{11}$$

where f_{end} is the crystal size distribution obtained at the end of the batch, which is evaluated by solving the population balance equation (PBE)

$$\frac{\mathrm{d}f(L,t)}{dt} + G\frac{\mathrm{d}f(L,t)}{dL} = f_{\mathrm{jet}}\left(L, t; v_{\mathrm{jet}}(t)\right) \tag{12}$$

where f_{jet} is the production rate of crystals from the impinging jet crystallizer in the units of #/μm s^{-1}. The distribution f_{jet} can be varied throughout the batch run by adjusting the jet velocity of the impinging jets. To illustrate the approach, the growth rate, G, in the batch aging vessel is held at a constant value by using supersaturation control, at a low enough supersaturation that secondary nucleation is negligible. It is also assumed that the mixing blade(s) and baffles are well-designed and the agitation intensity adjusted so that agglomeration and breakage in the batch aging vessel are negligible. Generalization of the approach to include secondary nucleation, agglomeration, and breakage increases the modeling and simulation requirements but is otherwise straightforward.

Eqn (12) can be solved using any PBE-solver; high-resolution finite-volume methods have the advantage of being easy to implement, having both a low numerical diffusion and dispersion compared to other methods for discretizing the PBE, and in being applicable to other crystallization phenomena such as aggregation, secondary nucleation, and breakage. For $G > 0$, the semidiscrete central scheme[24] discretizes the population balance equation along the crystal growth axis as:

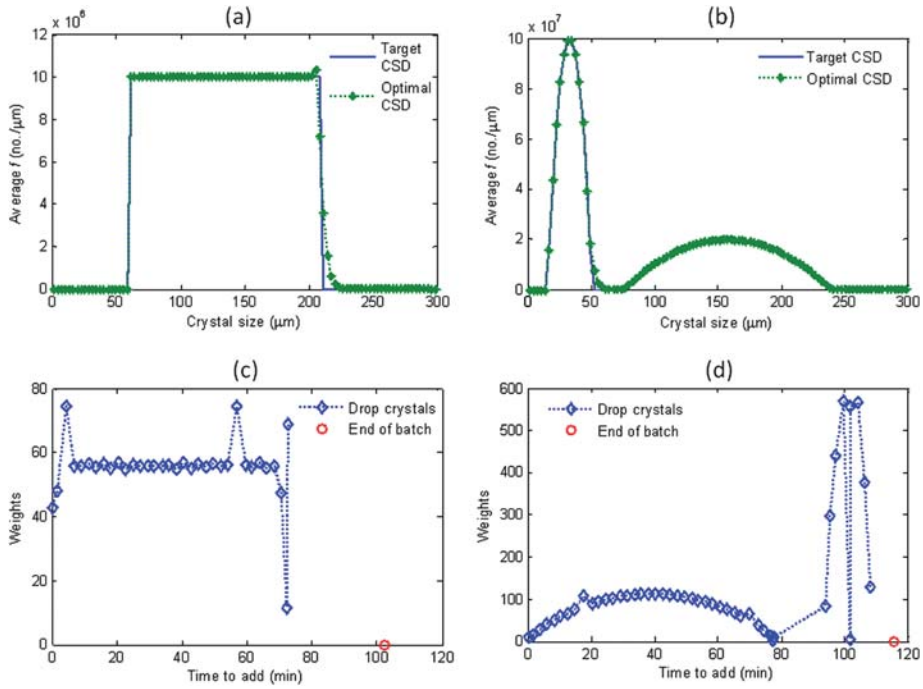

Fig. 5 Optimal crystal size distributions obtained by dropping crystals obtained from impinging jets into an aging vessel (growth rate = 2 μm min^{-1}) for **(a)** square and **(b)** bimodal target CSDs, with corresponding optimization weights **(c)** and **(d)**, respectively.

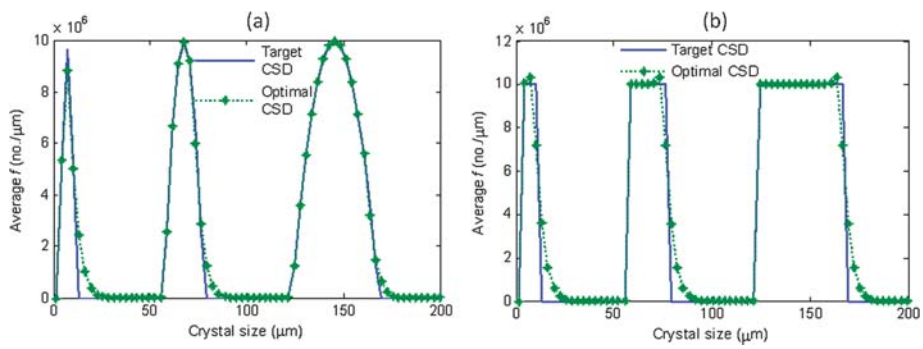

Fig. 6 Crystal size distributions obtained for various target distribution width and shape by dropping crystals obtained from impinging jets into an aging vessel for **(a)** smoothly varying trimodal target CSD, **(b)** sharp trimodal target CSD.

$$\frac{\mathrm{d}}{\mathrm{d}t}f_j(t) = -\frac{G}{\Delta L}\left\{\left[f_j(t) + \frac{\Delta L}{2}(f_L)_j(t)\right] - \left[f_{j-1}(t) + \frac{\Delta L}{2}(f_L)_{j-1}(t)\right]\right\} + f_{jet,j}(t) \qquad (13)$$

$$(f_L)_j := \mathrm{minmod}\left(\frac{f_j - f_{j-1}}{\Delta L}, \frac{f_{j+1} - f_{j-1}}{2\Delta L}, \frac{f_{j+1} - f_j}{\Delta L}\right)$$

where f_j is the cell-averaged population density, $f_{\mathrm{jet},j}$ is the cell-averaged population density from the impinging jet in the units of #/μm s^{-1}, and the minmod limiter is defined by

$$\mathrm{minmod}\,(\alpha_1, \alpha_2, \ldots) = \begin{cases} \min\limits_i \{\alpha_i\} & \text{if } \alpha_i > 0 \ \forall i \\ \max\limits_i \{\alpha_i\} & \text{if } \alpha_i < 0 \ \forall i \\ 0 & \text{otherwise} \end{cases} \qquad (14)$$

Eqn (13) can be solved by any solver of ordinary differential equations (*e.g.*, ode15s in Matlab 7.0.1).

The optimization (11), coupled with the population balance (12), defines the inlet velocity profile of the impinging jet crystallizer, $v_{\mathrm{jet}}(t)$. To solve the optimization (11), $v_{\mathrm{jet}}(t)$ was parameterized by treating the velocity as constant in variable time intervals with the following constraints:

$$v_{\mathrm{jet,min}} \leq v_{\mathrm{jet},j} \leq v_{\mathrm{jet,max}}$$
$$\Delta t_j \gg \text{time for impinging jets to reach steady state} \qquad (15)$$
$$(\approx 10 \times \text{residence time of the impinging jets})$$

where $v_{\mathrm{jet,min}}$ and $v_{\mathrm{jet,max}}$ are the minimum and maximum jet velocities for the impinging jets. The constraint that f_{jet} is obtained from an impinging jet crystallizer running at steady-state simplifies the formulation while having an insignificant effect on the optimal solution to eqn (11). This constraint is that the time interval should be long enough for f_{jet} to be nearly at its steady-state value throughout the time interval.

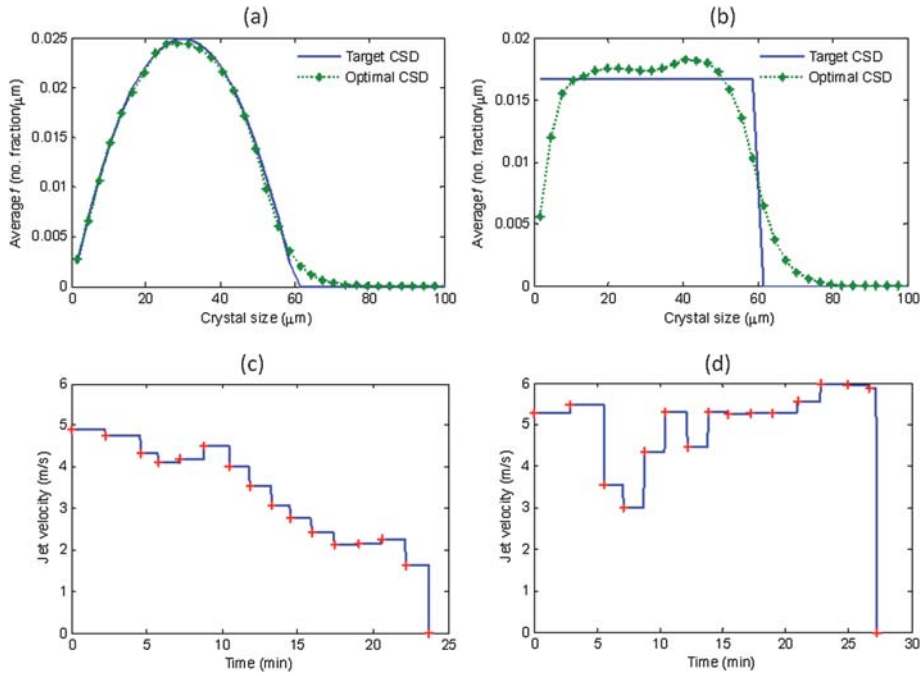

Fig. 7 Crystal size distributions obtained by optimal control of impinging jet velocity followed by growth in aging vessel for **(a)** smooth and **(b)** sharp target CSDs, with the corresponding optimal jet velocity profiles in **(c)** and **(d)**, respectively.

The residence time for an impinging jet is in the order of 0.01 s, hence, setting the second constraint as $\Delta t_j \geq 1$ s is sufficient.

Instead of using discrete velocities as in the previous two formulations, here f_{jet} is fit to a continuous function of jet velocity, *e.g.*, based on the distributions presented in Fig. 1 or measured for an impinging jet for a range of inlet velocity. Note that eqn (11) is written on a number fraction basis (that is, normalizing the number density by the total number of particles, 0th moment). The desired number of particles can be achieved by running multiple impinging jets in parallel or by changing the length of the run.

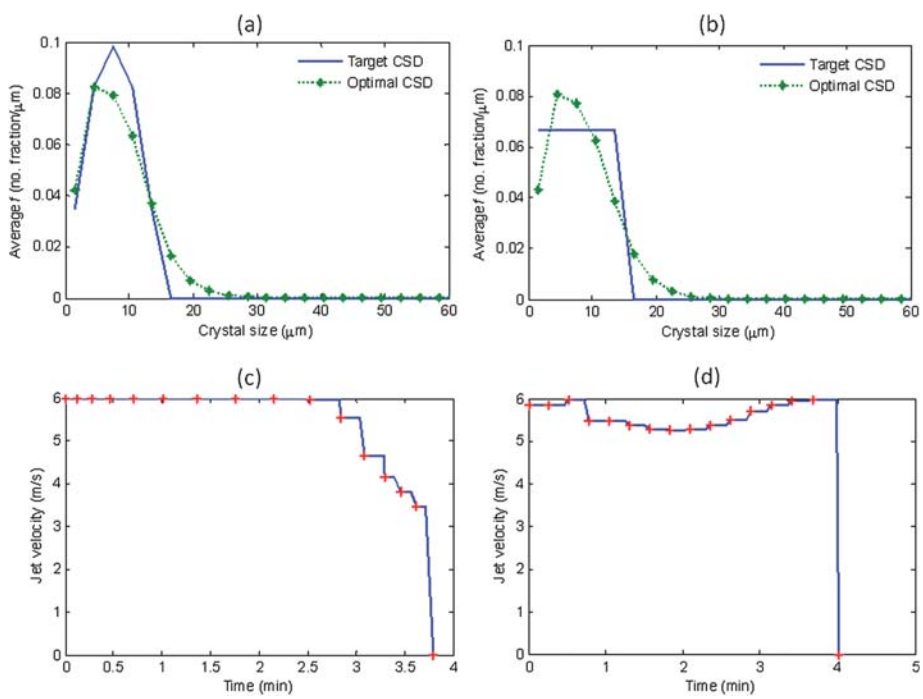

Fig. 8 Crystal size distributions obtained by optimal control of impinging jet velocity followed by growth in aging vessel for narrow **(a)** smooth and **(b)** sharp target CSDs, with the corresponding optimal jet velocity profiles in **(c)** and **(d)**, respectively.

Obtainable crystal size distributions

Here the above approach is applied to several target crystal size distributions. The growth rate used in the computations was 2 μm min^{-1} and the number of time intervals was 15. Fig. 7 shows that the optimal control of jet velocity is capable of achieving target distributions that have gradual changes in the number density along the crystal size axis. A limitation in the shape of the target crystal size distribution is that the number density must smoothly decrease towards its minimum and maximum size. Similar to the previous optimal seeding approach, the width of the target distribution is limited by the width of the crystal size distribution from the impinging jet crystallizer (compare Fig. 7a and 8).

Overall, the optimal control of impinging jet velocity in a combined impinging jet-batch aging vessel is effective in obtaining a much wider variety of crystal size distributions than for an impinging jet crystallizer on its own. The mean size of the crystals can be further increased by stopping the impinging jet crystallizer and allowing the crystals to grow in the aging vessel. Moreover, multi-modal distributions can be obtained by "switching off" the impinging jet crystallizer for a time period, which determines how far the modes are apart. The optimal velocity–time profile can be computed using the above optimal control formulation for each individual mode by shifting the target crystal size distribution of each mode to start at 0 μm.

Controllability and sensitivity analysis

The approach of combining impinging jets with an aging vessel to achieve crystals of desired size is commonly used in the pharmaceutical industry. However, the manipulation of jet velocity to target a specific crystal size distribution (CSD), as discussed above, has yet to be implemented. In this section, we will study, in further detail, the controllability and robustness of this process. Fig. 9 shows the variation of the CSD at the end of the batch of 30 min, where crystals from the impinging jet, operating at different jet velocities, are continuously added into the aging vessel with controlled constant growth rate of 2 μm min^{-1}. The plot illustrates that operating at different jet velocities does result in a range of size distributions at the end of the batch; given the dynamics of the CSD, these differences would increase as the batch time increases (and larger crystals are obtained). Hence there is significant controllability of the CSD obtained by varying the velocity of the impinging jets from low to high values.

As the CSD from the impinging jet converges at high velocities (see Fig. 1), the distribution at the end of the batch converges to the same distribution at sufficiently high velocities. This indicates that operating at high jet velocity gives very low sensitivity to disturbances in the jet velocity, while having much less controllability. Lower jet velocities result in higher controllability of the crystal size distribution, without having larger, but not excessively large, sensitivity to disturbances in jet velocity. To more fully understand the controllability of the process, various jet velocity profiles were applied to see their effects on the final CSD (see Fig. 10). As illustrated, the shape of the distribution varies widely with the jet velocity profile. For example, a narrower nearly-parabolic CSD was obtained for a linearly decreasing profile (second plot in Fig. 10), while a bimodal distribution was obtained for a convex parabolic profile in inlet velocity (fourth plot in Fig. 10). Thus, it is possible to optimize the control of the

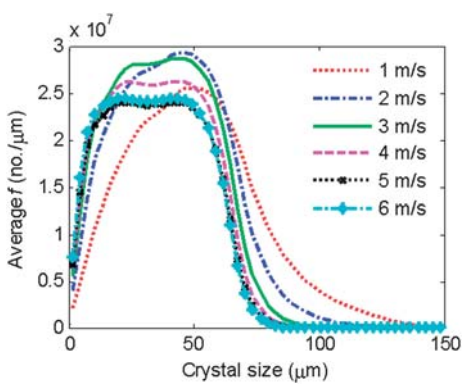

Fig. 9 CSD at the end of the batch with continuous addition of crystals from the impinging jet, with constant jet velocity, into a supersaturation-controlled tank (growth rate in tank = 2 μm min^{-1}, batch time = 30 min).

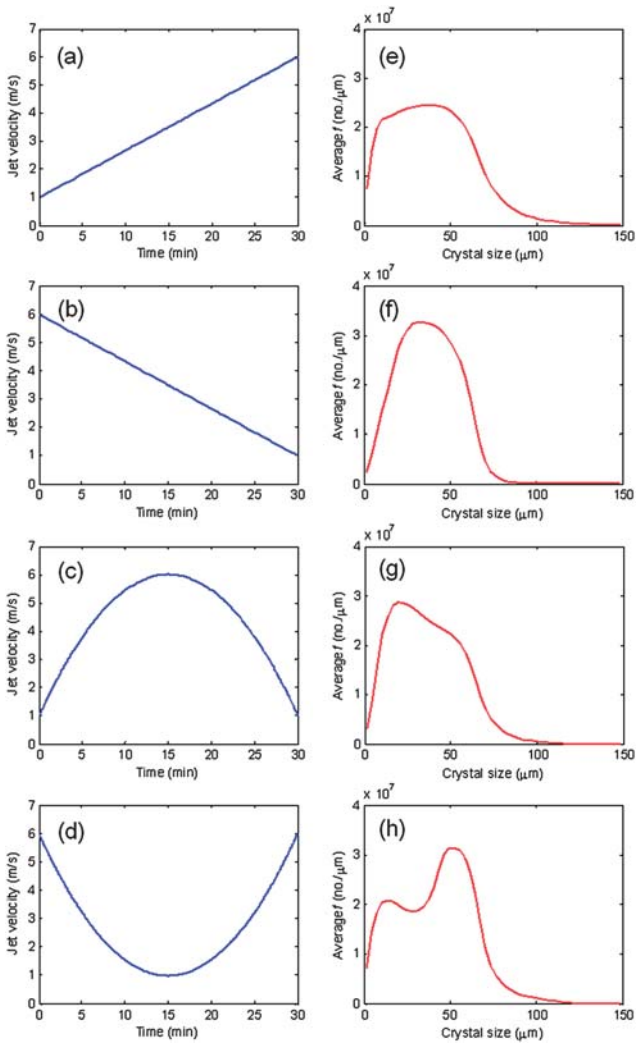

Fig. 10 **(a,b,c,d)** Impinging jet velocity profiles and **(e,f,g,h)** corresponding CSDs at the end of the batch in the aging vessel (growth rate in tank = 2 μm min^{-1}, batch time = 30 min).

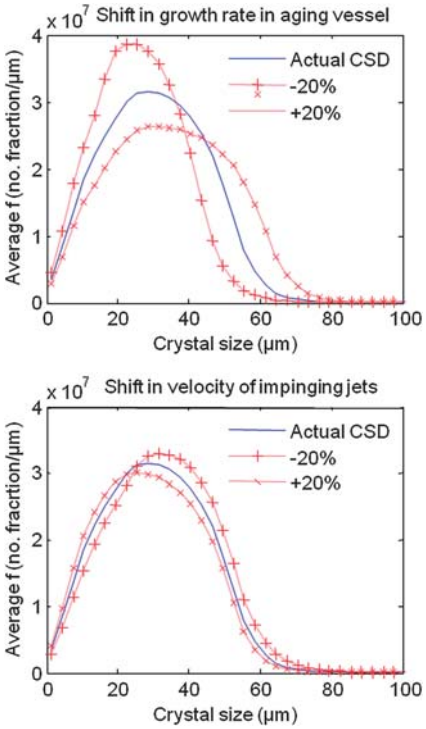

Fig. 11 Change in CSD due to perturbations of the growth rate in the aging vessel and the velocity of the impinging jets based on the optimal jet velocity profile in Fig. 7c.

jet velocity profile with time to produce crystals with a wide range in size distributions.

The sensitivity of the process to the variations in the supersaturation, hence growth rate, in the aging vessel and the jet velocity based on the optimal profile in Fig. 7 (left) is shown in Fig. 11. A slower growth rate results in a narrower size distribution, while a faster growth rate results in a wider size distribution. Note, however, that a 20% variation in growth rate corresponds to much larger variations in supersaturation than reported in past studies that demonstrated the robust feedback control of concentration in batch crystallization.[12,55] Since the solution concentration can be measured quite accurately and reproducibly,[12] such a large variation would be the result of a significant shift in the kinetics or solubility due to a shift in the contaminant concentrations in the chemical feedstocks. Variation in the solubility can be corrected with each new batch of chemical feedstocks by applying automated solubility measurement[12,27,55] at the production site.

Fig. 11 indicates that the crystal size distribution is relatively insensitive to shifts in jet velocity, since a 20% shift in inlet jet velocity is much larger than what would be obtained in practice. Comparing with Fig. 10 indicates that the overall shape of the jet velocity *versus* time profile has a greater impact on the final CSD, than the absolute values of the velocities of the jets. Overall, the analysis in this section shows that this control strategy is a promising approach for tailoring specific crystal size distributions.

Conclusions and future directions

This paper illustrates, in principle, three different approaches for the optimal control of an impinging jet crystallizer to produce crystals with a target crystal size distribution. The results indicate a great increase in the controllability in targeting crystal size distributions for an impinging jet coupled with an aging vessel. The main limitation is that the minimum width of the distribution is limited by the narrowest crystal size distribution produced from the impinging jet. The key inputs into the optimization process are:

1. The crystal size distributions as a function of jet velocity from the impinging jet crystallizer, which can be obtained from experiments[31] or simulations validated by experiments.[53]

2. The growth kinetics of the crystallization system so as to determine the supersaturation profile to achieve the desired growth rate. Unlike nucleation kinetics, crystal growth rates can be estimated or directly measured with high accuracy.[9,15,29,43,48,54]

The results indicate that the optimal control of impinging jet crystallizers is a promising strategy to produce a target crystal size distribution, providing a level of CSD control far beyond what is achievable using the batch and continuous "well-mixed" vessels that currently dominate the industry. This level of CSD control is good enough to consider the development of a systematic approach for crystal product engineering, in which a desired crystal product is determined by product design,[10] when the approach taken in this paper is used to design the process to manufacture that desired product. The next step is to implement the control strategies on laboratory experiments to fully evaluate the feasibility of the approaches. Constraints identified from experiments can be incorporated into the optimization algorithms and further improvements can be explored.

Acknowledgements

Financial support is acknowledged from the Singapore Agency for Science, Technology, and Research.

References

1 D. J. am Ende and S. J. Brenek, *Am. Pharm. Rev.*, 2004, **7**, 98–104.
2 D. J. am Ende, T. C. Crawford and N. P. Weston, U.S. patent 6,558,435, 2003.
3 A. Bauer-Brandl, *Int. J. Pharm.*, 1996, **140**, 195–206.
4 W. Beckmann, *Org. Process Res. Dev.*, 2000, **4**, 372–383.
5 P. W. Bell, A. P. Stephens, C. B. Roberts and S. R. Duke, *Exp. Fluids*, 2005, **38**, 708–719.
6 R. D. Braatz, *Annu. Rev. Control*, 2002, **26**, 87–99.
7 K. L. Choong and R. Smith, *Chem. Eng. Sci.*, 2004, **59**, 313–327.
8 S. H. Chung, D. L. Ma and R. D. Braatz, *Can. J. Chem. Eng.*, 1999, **77**, 590–596.
9 S. H. Chung, D. L. Ma and R. D. Braatz, *Chemom. Intell. Lab. Syst.*, 2000, **50**, 83–90.
10 R. Costa, G. D. Moggridge and P. M. Saraiva, Chemical product engineering: An emerging paradigm within chemical engineering, *AIChE J.*, 2006, **52**, 1976–1986.
11 R. Dauer, J. E. Mokrauer and W. J. McKeel, Dual jet crystallizer apparatus. U.S. patent 5,578,279, 1996.
12 M. Fujiwara, P. S. Chow, D. L. Ma and R. D. Braatz, Paracetamol crystallization using laser backscattering and ATR-FTIR spectroscopy: Metastability, agglomeration, and control, *Cryst. Growth Des.*, 2002, **2**, 363–370.
13 M. Fujiwara, Z. K. Nagy, J. W. Chew and R. D. Braatz, First-principles and direct design approaches for the control of pharmaceutical crystallization, *J. Process Control*, 2005, **15**, 493–504.
14 H. Grön, A. Borissova and K. J. Roberts, In-process ATR-FTIR spectroscopy for closed-loop supersaturation control of a batch crystallizer producing monosodium glutamate crystals of defined size, *Ind. Eng. Chem. Res.*, 2003, **42**, 198–206.

15 R. Gunawan, D. L. Ma, M. Fujiwara and R. D. Braatz, Identification of kinetic parameters in multidimensional crystallization processes, *Int. J. Mod. Phys. B*, 2002, **16**, 367–374.
16 M. Henczka, J. Baldyga and B. Y. Shekunov, Particle formation by turbulent mixing with supercritical antisolvent, *Chem. Eng. Sci.*, 2005, **60**, 2193–2201.
17 D. Jagadesh, N. Kubota, M. Yokota, N. Doki and A. Sato, Seeding effect on batch crystallization of potassium sulfate under natural cooling mode and a simple design method of crystallizer, *J. Chem. Eng. Jpn.*, 1999, **32**, 514–520.
18 D. Jagadesh, N. Kubota, M. Yokota, A. Sato and N. S. Tavare, Large and mono-sized product crystals from natural cooling mode batch crystallizer, *J. Chem. Eng. Jpn.*, 1996, **29**, 865–873.
19 B. K. Johnson and R. K. Prud'homme, Flash nanoprecipitation of organic actives and block copolymers using a confined impinging jets mixer, *Aust. J. Chem.*, 2003, **56**, 1021–1024.
20 A. G. Jones and J. W. Mullin, Programmed cooling crystallization of potassium sulfate solutions, *Chem. Eng. Sci.*, 1974, **29**, 105–118.
21 J. Jung and M. Perrut, Particle design using supercritical fluids: Literature and patent survey, *J. Supercrit. Fluids*, 2001, **20**, 179–219.
22 S. Kim, B. Lotz, M. Lindrud, K. Girard, T. Moore, K. Nagarajan, M. Alvarez, T. Lee, F. Nikfar, M. Davidovich, S. Srivastava and S. Kiang, Control of the particle properties of a drug substance by crystallization engineering and the effect on drug product formulation, *Org. Process Res. Dev.*, 2005, **9**, 894–901.
23 N. Kubota, N. Doki, M. Yokota and D. Jagadesh, Seeding effect on product crystal size in batch crystallization, *J. Chem. Eng. Jpn.*, 2002, **35**, 1063–1071.
24 A. Kurganov and E. Tadmor, New high-resolution central schemes for nonlinear conservation laws and convection-diffusion equations, *J. Comput. Phys.*, 2000, **160**, 241–282.
25 J. H. Kwon and C. W. Kim, A novel insulin microcrystals preparation using a seed zone method, *J. Cryst. Growth*, 2004, **263**, 536–543.
26 M. D. Lindrud, S. Kim and C. Wei, *Sonic impinging jet crystallization apparatus and process*. Bristol-Myers Squibb Company. U.S. patent 6,302,958, 2001.
27 V. Liotta and V. Sabesan, Monitoring and feedback control of supersaturation using ATR-FTIR to produce an active pharmaceutical ingredient of a desired crystal size, *Org. Process Res. Dev.*, 2004, **8**, 488–494.
28 B. L. M. Lung-Somarriba, M. Moscosa-Santillan, C. Porte and A. Delacroix, Effect of seeded surface area on crystal size distribution in glycine batch cooling crystallization: a seeding methodology, *J. Cryst. Growth*, 2004, **270**, 624–632.
29 D. L. Ma and R. D. Braatz, Robust identification and control of batch processes, *Comput. Chem. Eng.*, 2003, **27**, 1175–1184.
30 D. L. Ma, D. K. Tafti and R. D. Braatz, Optimal control and simulation of multidimensional crystallization processes, *Comput. Chem. Eng.*, 2002, **26**, 1103–1116.
31 A. J. Mahajan and D. J. Kirwan, Micromixing effects in a two-impinging-jets precipitator, *AIChE J.*, 1996, **42**, 1801–1814.
32 D. L. Marchisio, L. Rivautella and A. A. Barresi, Design and scale-up of chemical reactors for nanoparticle precipitation, *AIChE J.*, 2006, **52**, 1877–1887.
33 A. Martin and M. J. Cocero, Numerical modeling of jet hydrodynamics, mass transfer, and crystallization kinetics in the supercritical antisolvent (SAS) process, *J. Supercrit. Fluids*, 2004, **32**, 203–219.
34 M. Midler, E. L. Paul, E. F. Whittington, M. Futran, P. D. Liu, J. Hsu and S.-H. Pan, Crystallization method to improve crystal structure and size. U.S. patent 5,314,506, 1994.
35 K. W. Morton and D. F. Mayers, *Numerical Solution of Partial Differential Equations*, Cambridge University Press, Cambridge, U.K., 1994.
36 G. Muhrer, M. Mazzotti and M. Muller, Gas antisolvent recrystallization of an organic compound. Tailoring product PSD and scaling-up, *J. Supercrit. Fluids*, 2003, **27**, 195–203.
37 L. M. Nagao, S. Lyapustina, M. K. Munos and M. D. Capizzi, Aspects of particle science and regulation in pharmaceutical inhalation drug products, *Cryst. Growth Des.*, 2005, **5**, 2261–2267.
38 Z. K. Nagy, M. Fujiwara and R. D. Braatz, Modelling and control of combined cooling and antisolvent crystallization processes, *J. Process Control*, 2008, **18**, 856–864.
39 Z. K. Nagy, J. W. Chew, M. Fujiwara and R. D. Braatz, Comparative performance of concentration and temperature controlled batch crystallizations, *J. Process Control*, 2008, **18**, 399–407.
40 I. Pasquali, R. Bettini and F. Giordano, Solid-state chemistry and particle engineering with supercritical fluids in pharmaceutics, *Eur. J. Pharm. Sci.*, 2006, **27**, 299–310.
41 E. L. Paul, H.-H. Tung and M. Midler, Organic crystallization processes, *Powder Technol.*, 2005, **150**, 133–143.
42 N. Rasenack, H. Steckel and B. W. Muller, Micronization of anti-inflammatory drugs for pulmonary delivery by a controlled crystallization process, *J. Pharm. Sci.*, 2003, **92**, 35–44.
43 J. B. Rawlings, S. M. Miller and W. R. Witkowski, Model Identification and Control of Solution Crystallization Processes - a Review, *Ind. Eng. Chem. Res.*, 1993, **32**, 1275–1296.
44 S. Rohani, S. Horne and K. Murthy, Control of product quality in batch crystallization of pharmaceuticals and finechemicals. Part 1: Design of the crystallization process and the effect of solvent, *Org. Process Res. Dev.*, 2005, **9**, 858–872.
45 S. Rohani, S. Horne and K. Murthy, Control of product quality in batch crystallization of pharmaceuticals and fine chemicals. Part 2: External control, *Org. Process Res. Dev.*, 2005, **9**, 873–883.
46 B. Y. Shekunov and P. York, Crystallization processes in pharmaceutical technology and drug delivery design, *J. Cryst. Growth*, 2000, **211**, 122–136.
47 B. Steffen, K. P. Muller, M. Komenda, R. Koppmann and A. Schaub, A new mathematical procedure to evaluate peaks in complex chromatograms, *J. Chromatogr., A*, 2005, **1071**, 239–246.
48 T. Togkalidou, H.-H. Tung, Y. Sun, A. T. Andrews and R. D. Braatz, Parameter estimation and optimization of a loosely bound aggregating pharmaceutical crystallization using in situ infrared and laser backscattering measurements, *Ind. Eng. Chem. Res.*, 2004, **43**, 6168–6181.
49 J. R. Torres-Lapasio, J. J. Baeza-Baeza and M. C. Garcia-Alvarez-Coque, A model for the description, simulation, and deconvolution of skewed chromatographic peaks, *Anal. Chem.*, 1997, **69**, 3822–3831.
50 G. Vivo-Truyols, J. R. Torres-Lapasio, A. M. van Nederkassel, Y. Vander Heyden and D. L. Massart, Automatic program for peak detection and deconvolution of multi-overlapped chromatographic signals - Part II: Peak model and deconvolution algorithms, *J. Chromatogr., A*, 2005, **1096**, 146–155.
51 J. D. Ward, D. A. Mellichamp and M. F. Doherty, Choosing an operating policy for seeded batch crystallization, *AIChE J.*, 2006, **52**, 2046–2054.
52 X. Y. Woo, Z. K. Nagy, R. B. H. Tan and R. D. Braatz, Adaptive concentration control of cooling and antisolvent crystallization with laser backscattering measurement, *Cryst. Growth Des.*, 2009, **9**, 182–191.
53 X. Y. Woo, R. B. H. Tan and R. D. Braatz, Modeling and computational fluid dynamics-population balance equation-micromixing simulation of impinging jet crystallizers, *Cryst. Growth Des.*, 2009, **9**, 156–164.
54 J. Worlitschek and M. Mazzotti, Model-based optimization of particle size distribution in batch-cooling crystallization of paracetamol, *Cryst. Growth Des.*, 2004, **4**, 891–903.
55 G. X. Zhou, M. Fujiwara, X. Y. Woo, E. Rusli, H.-H. Tung, C. Starbuck, O. Davidson, Z. Ge and R. D. Braatz, Direct design of pharmaceutical antisolvent crystallization through concentration control, *Cryst. Growth Des.*, 2006, **6**, 892–898.